Received: 23 December 2020 | Revised: 26 January 2021 | Accepted: 27 January 2021

DOI: 10.1002/ardp.202000486

FULL PAPER

ARCH PHARM DPhG
Archiv der Pharmazie

Synthesis, in silico, and in vitro studies of novel dopamine D_2 and D_3 receptor ligands

Milica Elek[1] | Nemanja Djokovic[2] | Annika Frank[1] | Slavica Oljacic[2] | Aleksandra Zivkovic[1] | Katarina Nikolic[2] | Holger Stark[1]

[1]Institute of Pharmaceutical and Medicinal Chemistry, Heinrich Heine University Düsseldorf, Universitaetsstr. 1, Duesseldorf, NRW, Germany

[2]Department of Pharmaceutical Chemistry, Faculty of Pharmacy, University of Belgrade, Belgrade, Serbia

Correspondence
Holger Stark, Heinrich Heine University Düsseldorf, Institute of Pharmaceutical and Medicinal Chemistry, Universitaetsstr. 1, 40225 Duesseldorf, Germany.
Email: stark@hhu.de

Funding information
Deutscher Akademischer Austausch Dienst, Grant/Award Number: Milica Elek; Ministarstvo Prosvete, Nauke i Tehnološkog Razvoja, Grant/Award Number: UB Contract No. 451-03-68/2020-14/200161; European Cooperation in Science and Technology, Grant/Award Numbers: CA15135, CA18133, CA18240; Deutsche Forschungsgemeinschaft, Grant/Award Number: INST 208/664-1 FUGG

Abstract

Dopamine is an important neurotransmitter in the human brain and its altered concentrations can lead to various neurological diseases. We studied the binding of novel compounds at the dopamine D_2 (D_2R) and D_3 (D_3R) receptor subtypes, which belong to the D_2-like receptor family. The synthesis, in silico, and in vitro characterization of 10 dopamine receptor ligands were performed. Novel ligands were docked into the D_2R and D_3R crystal structures to examine the precise binding mode. A quantum mechanics/molecular mechanics study was performed to gain insights into the nature of the intermolecular interactions between the newly introduced pentafluorosulfanyl (SF_5) moiety and D_2R and D_3R. A radioligand displacement assay determined that all of the ligands showed moderate-to-low nanomolar affinities at D_2R and D_3R, with a slight preference for D_3R, which was confirmed in the in silico studies. *N*-{4-[4-(2-Methoxyphenyl)piperazin-1-yl]butyl}-4-(pentafluoro-λ6-sulfanyl)benzamide (**7i**) showed the highest D_3R affinity and selectivity (pK_i values of 7.14 [D_2R] and 8.42 [D_3R]).

KEYWORDS
D_2 receptor, D_3 receptor, ligands, pentafluorosulfanyl, QM/MM

1 | INTRODUCTION

Disorders as a result of neurodegenerative diseases, such as schizophrenia, Parkinson's disease, Alzheimer's disease, affective disorder, and addictive behavior, have been connected to altered concentrations of neurotransmitters in the human brain, especially dopamine. During the 1960s, dopamine was recognized as an independent neurotransmitter in addition to other well-known catecholamines.[1] Biosynthesis of dopamine, epinephrine, and norepinephrine starts from tyrosine. Dopaminergic neurons do not contain dopamine β-hydroxylase enzymes that convert dopamine to norepinephrine. Catabolic reactions of dopamine include degradation by monoamine oxidase B,[2] catecholamine-*O*-methyl transferase, as well as partly by monoamine oxidase A.[2–5] On the basis of amino-acid sequences and similarity in signal transduction, dopamine receptors are divided into two different classes: dopamine D_1-like receptors that include D_1 and D_5 receptors and dopamine D_2-like receptors that include D_2, D_3, and D_4 receptors.[6–8] All dopamine receptor subtypes belong to the rhodopsin-like A class of the largest group of G-protein-coupled receptors (GPCR), characterized by the presence of seven transmembrane domains. D_1-like receptors express a long carboxyl and D_2-like receptors express a short carboxy tail, which is located intracellularly in both receptor subtypes.[9] D_1-like receptors signal through $G_{\alpha s}$ protein and enhance the production of cAMP, whereas D_2-like receptors activate $G_{\alpha i}$ that inhibits the production cAMP

in the cell.[10,11] Dopamine D_2 receptor (D_2R) has also been implicated in the G protein-independent GPCR signaling, involving mediation with β-arrestin 1 and β-arrestin 2, which scaffold the different pathways.[12] D_1-like receptors are mainly located in the *corpus striatum*, *nucleus accumbens*, *substantia nigra*, olfactory bulb, and frontal cortex.[13,14] D_2-like receptors are mostly found in *substantia nigra*, hypothalamus, amygdala, and hippocampus,[15] and their density, regional distribution, and synaptic response are affected by various neurological diseases,[16] stress, or drug abuse.[17] Majority of commercially available D_2-like receptor ligands have severe side effects due to their low selectivity to the receptors of interest and high affinity toward other off-target receptors. To counter this, efforts have been centered around the design and synthesis of selective D_2-like receptor ligands.[18] The main challenges in developing novel ligands as potent pharmacological tools in the treatment of diseases with altered concentration of dopamine are high homology between receptors subtypes (up to 88% of D_2R and D_3 receptor [D_3R] in structurally conserved regions)[19] and almost identical orthosteric binding site (OBS) interaction within two receptors subtypes.[20–22] Since its revelation, the D_3R has been a target of interest in potential pharmacotherapy of addiction and schizophrenia,[23] due to its relatively focal localization and its expression in drug-exposed brains.[24] In addition, it has also emerged as a new potential target in the treatment of Parkinson's disease.[25] Although all of the dopamine receptor subtypes show a high level of similarity, it has been shown that dopamine itself has a 100-fold higher affinity at D_3R when compared with those at D_1R or D_2R.[26] In addition, D_3R messenger RNA, which is localized predominantly in the *islands of Calleja* and *nucleus accumbens* in healthy humans,[27] could be a potential biomarker in early-stage Parkinson's patients.[28] Therefore, serious efforts have been made to find potent, novel, and selective D_3R ligands.

A general pharmacophore of D_3R antagonists has been described in the early 2000s.[29] It contains four regions: The aromatic, the H-bond acceptor, the linker, and the amine regions. Piperazine has been described as a promising moiety for binding and positioning into OBS of D_3R,[30–32] and therefore, is a structural part not only of many commercially available drugs (e.g., lurasidone and cariprazine)[33–36] but also of preclinical and clinical candidates.[37–39] The prototype of D_3R partial agonizts is BP897 (Figure 1).[40,41] BP897, which was developed for the treatment of cocaine abuse, is a potent D_3R ligand (K_i = 0.92 nM) that served as a lead compound for many synthesized ligands in this study. In addition, it has been established that ligands containing 4-(2-methoxyphenyl)piperazino and 4-(2,3-dichlorophenyl)piperazino moieties could have beneficial properties for D_2-like receptor binding[21] and lead to the development of new potent selective ligands.[42–44] These moieties have, therefore, been used in the synthesis of all 10 reported compounds. A novel thermally and chemically stable pentafluorosulfanyl (SF_5) moiety that displays high values of electronegativity and lipophilicity[45,46] was introduced to compare its effects on affinity and selectivity toward receptors of interest. Due to these beneficial chemical properties, SF_5 can be used as a valuable bioisosteric replacement of the trifluoromethyl and under special circumstances of *tert*-butyl or nitro group.[47] Therefore, our main aim is to develop, synthesize, and in vitro and in silico characterize potent dopamine D_2R and D_3R ligands, which could be further optimized and in vivo evaluated.

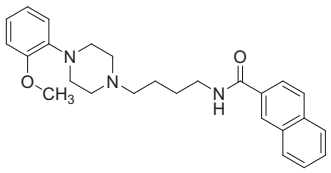

FIGURE 1 Chemical structure of the lead compound BP897

2 | RESULTS AND DISCUSSION

2.1 | Chemistry

To obtain amines **6a–e**, two different synthetic methods have been used. In the first synthetic approach (Route I), compound **1a** has been alkylated with *N*-(ω-bromoalkyl)phthalimide derivatives **2a–c** to obtain protected amines **4a–c**. Consequently, hydrazine as a cleaving reagent has been used for the deprotection of amines. To obtain higher yields as well as to decrease costs of the synthesis, the second synthetic approach (Route II) was introduced, where compounds **1a,b** have been alkylated with 4-bromobutanenitrile (**3a**) and 5-bromovaleronitrile (**3b**), respectively. Reduction of obtained nitriles led to crude amines **6c–e**. Then, the primary amines **6a–e** were coupled with a corresponding activated carboxylic acid to amides **7a–j**. Both approaches are shown in Scheme 1.

2.2 | Pharmacology

The affinity at human isoform dopamine $D_{2short}R$ and D_3R was determined by radioligand displacement assays, as described before.[48–50] In brief, radioligand displacement studies on membranes prepared from CHO-K1 cells expressing human dopamine $D_{2short}R$ or D_3R have been performed using [^{3}H]spiperone as a radioligand and haloperidol as a standard for unspecific binding. The binding affinities of the synthesized compounds with the corresponding confidence intervals (CIs) as well as the selectivity index (SI) are shown in Table 1.

2.3 | Molecular docking

Molecular docking was used to access the binding modes of the synthesized ligands and to obtain atomistic insight into the observed inhibitory activities. All synthesized compounds were docked into binding pockets of the cocrystal structures of D_2R and D_3R. In addition, docking scores were evaluated in terms of correlation with observed binding affinities.

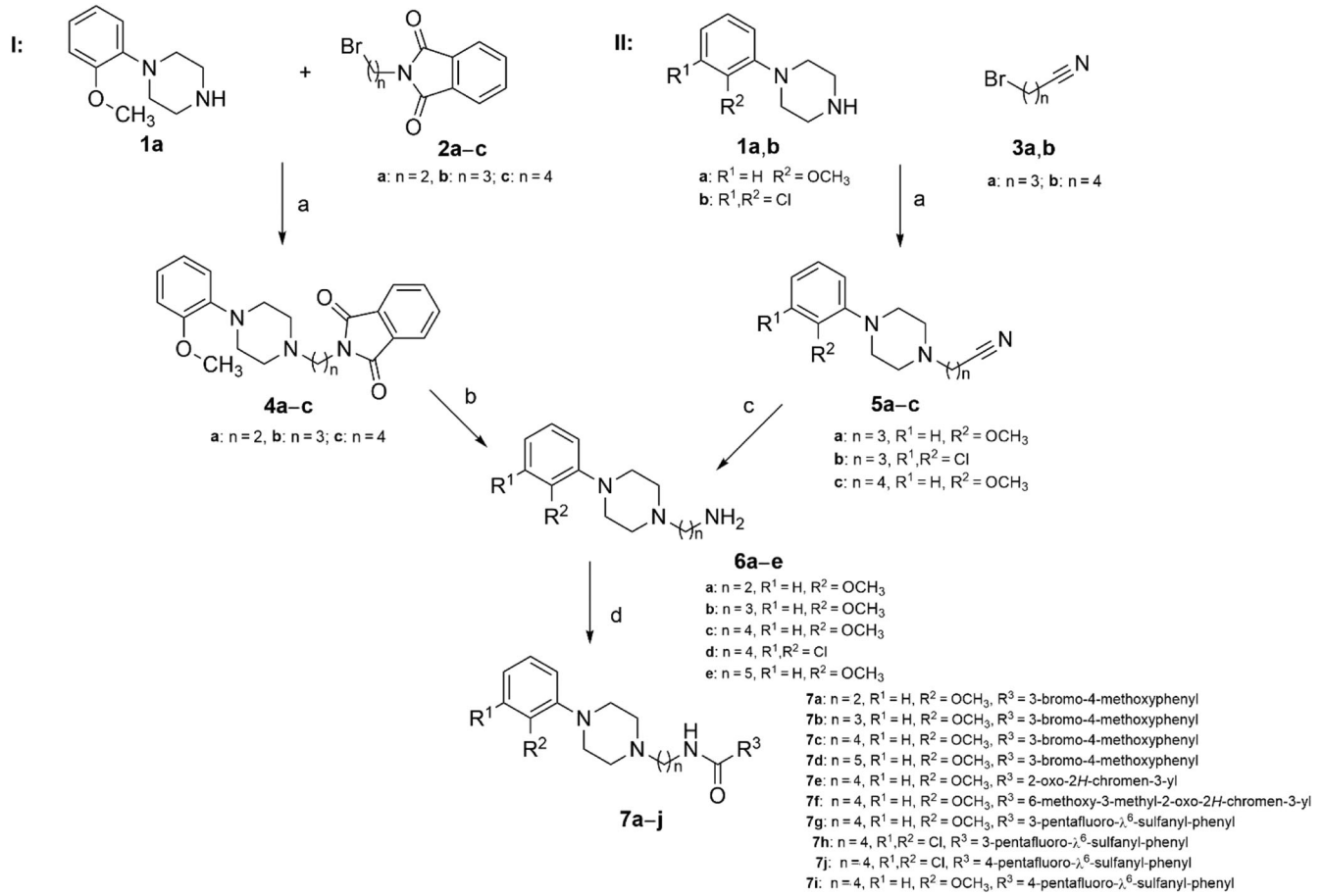

SCHEME 1 Synthesis of compounds **7a–j**. Reagents and conditions: (a) K_2CO_3, KI, reflux 16 h; (b) H_2NH_2N, MeOH, reflux, 2 h; 2 M HCl, reflux, 1 h; (c) Raney-Ni, NH_3/MeOH, H_2 5 bar,12 h; (d) HOOC-R^3, HOBt, EDC, R.T., 16 h

2.3.1 | Docking in D_3R active site

All ligands were docked into the D_3R cocrystal structure (PDB ID: 3PBL) in complex with eticlopride[21,51] (a potent D_2R/D_3R antagonist) according to the protocol described in Section 4. The docking protocol was validated through redocking of eticlopride and calculation of heavy atoms RMSD (root mean square deviation), which typically should not exceed 2 Å[52] (RMSD eticlopride = 0.67 Å, Figure S1). Pearson's correlation coefficient (R^2) and Spearman's rank correlation coefficient (r_s) were used to access the correlation between docking and experimental results. Calculated docking scores for our set of ligands significantly correlated with experimental affinity (pK_i) measurements for D_3R ($R^2 = 0.92$, $r_s = 0.97$, Table S1). High correlation coefficient values justified the reliability of obtained binding modes for ligands.

Predicted binding modes indicate that phenylpiperazine moiety (arylamine head) binds to OBS, with the rest of the structures (arylamide/coumarine tails) extending to the extracellular vestibule/second binding pocket (SBP)[21] (Figures 2a and S2). This is in agreement with previous docking studies of structurally related compounds.[52,53] For all studied ligands, highly conserved residue Asp $110^{3.32}$ (OBS) formed a salt bridge with positively charged nitrogen from piperazine. This salt bridge interaction is believed to be crucial in binding of ligands at the OBS of D_3R, which is in agreement with our docking results.[21]

Comparison of interacting modes between eticlopride and ligand **7i** (Figure 1a), as the representative with the highest affinity to the D_3R, indicates a similar interaction profile in OBS. Interestingly, pi–alkyl interaction between arylamine heads of the studied ligands and Cys $114^{3.36}$, absent in the cocrystal structure with eticlopride (Figure 1a), signifies the importance of this residue in the binding of our series of phenylpiperazine ligands. Residue Cys $114^{3.36}$ (OBS) has been characterized as important for binding of haloperidol in recent mutagenesis experiments. According to the predicted poses of docked ligands, arylamide/coumarine tails are bound to the extracellular vestibule shaped by Tyr $36^{1.39}$, Val $86^{2.60}$, Leu $89^{2.63}$, Glu $90^{2.64}$, Gly 93, and Ser $366^{7.35}$ (Figures 1a and S2). Tyr $36^{1.39}$ and Glu $90^{2.64}$ have been characterized in recent combined large-scale high-throughput molecular dynamics study and mutagenesis study as important for binding of GSK598809 (dual D_2R/D_3R antagonist), which further validates predicted binding modes.[54]

TABLE 1 Synthesized ligands and their in vitro affinity data

Name	Structure	MW	K_i (D_2R) (nM) (95% CI)	K_i (D_3R) (nM) (95% CI)	SI (D_2/D_3)
Haloperidol (reference compound)	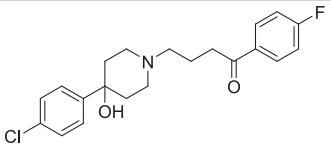	375.9	2.61 (2.02; 3.39)	13.5 (10.4; 17.4)	0.2
7a	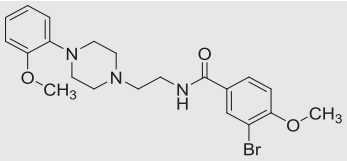	448.4	105.1 (76.5; 144)	184 (99.7; 339)	0.6
7b	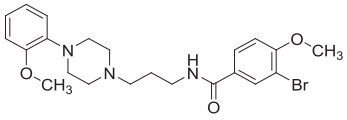	462.4	152 (68.2; 338);	127 (28.1; 570)	1.2
7c	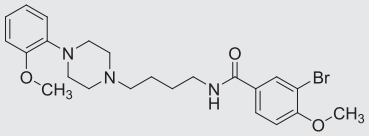	476.4	9.45 (4.71; 19.0)	5.67 (1.88; 17.0)	1.7
7d	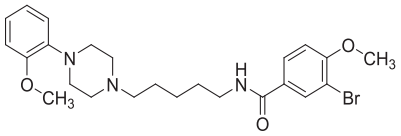	490.4	13.4 (9.16; 19.7)	30.7 (12.6; 75.3)	0.4
7e	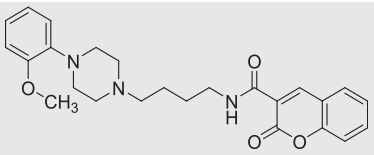	435.5	65.5 (42.6; 101)	9.04 (6.87; 11.9)	7.2
7f	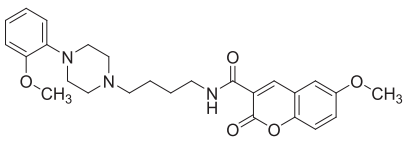	465.6	63.4 (36.5; 110)	3.90 (1.57; 9.70)	16.3
7g	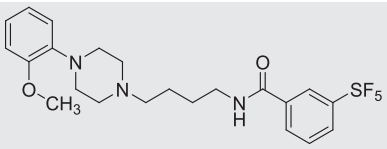	493.5	54.3 (28.2; 105)	4.96 (2.51; 9.79)	10.9
7h	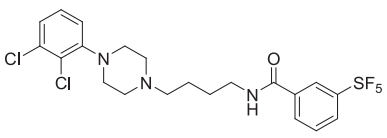	532.2	62.3 (25.5; 152)	9.34 (5.45; 16.0)	13.3
7i	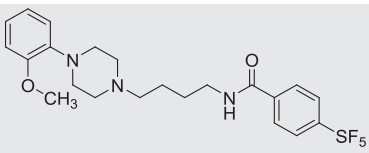	493.5	72.3 (31.3; 167)	3.52 (1.46; 8.74)	20.5
7j	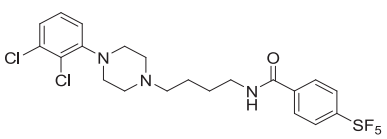	532.2	163 (90.2; 293)	12.2 (6.69; 22.4)	6.7

Abbreviations: MW, molecular weight; SI, selectivity index.

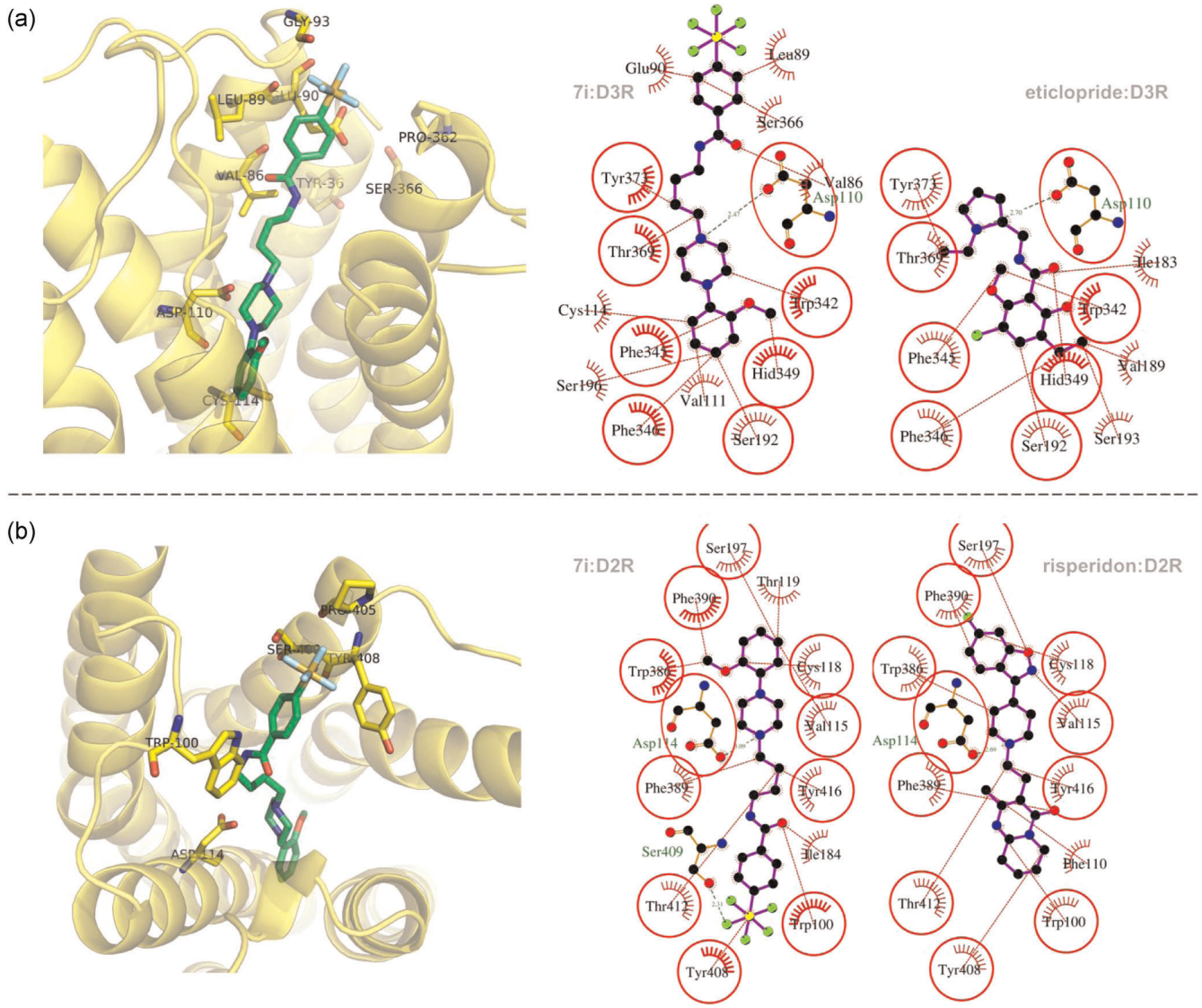

FIGURE 2 Docking results of **7i** into the binding site of (a) D_3R and (b) D_2R. The left side of the figure corresponds to the three-dimensional (3D) representation of binding sites, whereas the right side of the figure corresponds to the comparative 2D interaction plots obtained for **7i** and cocrystal ligands (a, eticlopride; b, risperidone). Encircled residues on 2D interaction plots represent residues that are engaged in interactions with both ligands

2.3.2 | Docking in the D_2R active site

Atypical antipsychotic risperidone was correctly redocked in PDB ID: 6CM4 using the docking protocol described in Section 4 (heavy atoms RMSD 0.62 Å, Figure S3). A correlation between docking scores and experimental affinity (pK_i) ($R^2 = 0.32$, $r_s = 0.73$, Table S1) was not as good as for D_3R docking, but still under the range of medium correlations expected for docking studies.[55] A possible explanation for better correlation found in D_3R docking study could be found in recently reported higher flexibility of D_2R's extended binding pocket (EBP) as compared with the related part of D_3R. This flexibility was previously seen as the main reason why structure-based drug discovery campaigns were less successful in the case of D_2R.[56] All the studied ligands showed a similar binding mode to cocrystalized risperidon: arylamino head was docked into OBS, whereas arylamido/coumarine tail was docked into EBP (Figures 2b and S4).[22] Comparison of two-dimensional (2D) interaction profiles for risperidone and **7i** (representative with the highest selectivity index) indicates high similarity in binding profiles (Figure 2b). A salt bridge was observed between Asp114$^{3.32}$ and positively charged nitrogen from piperazine. This interaction was previously characterized as fundamental for binding to the OBS of D_2R. In addition, two recently reported docking studies on D_2R cocrystal structure further support our results regarding predicted binding modes of ligands.[57,58]

In series of *p*-monosubstituted SF_5 derivatives (**7i** and **7j**), *m*-monosubstituted SF_5 derivatives (**7g** and **7h**), and *p*,*m*-disubstituted derivative with the same linker length (**7c**), docking results indicate that

m-substitution is responsible for achieving an optimal interaction with Tyr 408$^{7.34}$ (Figure S5). Our results indicate that *p*-substitution with a voluminous substituent (e.g., SF_5 moiety) in series of similar compounds (four-methylene groups linker) tends to decrease affinity toward D_2R due to steric hindrance, whereas it does not affect, to a larger extent, affinity at D_3R. This is in accordance with experimental findings regarding the distances between OBS and EBS in D_2R and D_3R, where this distance is longer in D_3R.[21,56]

2.4 | Quantum mechanics/molecular mechanics (QM/MM) calculations

Pentafluorosulfanyl moiety is a relatively novel moiety in medicinal chemistry and only a limited number of compounds containing this moiety have been studied in interaction with biological systems.[47] Furthermore, atomistic details on the interaction between the SF_5 group and biological target molecules remain enigmatic, as no co-crystal/nuclear magnetic resonance (NMR) structures have been described so far. Also, there is a lack of detailed molecular modeling studies on SF_5 ligands. To the best of the authors' knowledge, the most common force fields used for biomolecular simulations (e.g., CHARMM and AMBER sets of force fields) do not recognize this moiety or this specific hypervalent sulfur atom type, which hinders the application of classical molecular dynamics simulations. Hybrid QM/MM approaches, where ligand and interacting residues are treated quantum mechanically, whereas the rest of the system (e.g., membrane, solvent, noninteracting residues, etc.) is treated classically, represent viable alternative to overcome limitations of current force fields in studying noncovalent interactions between SF_5 and the biomolecule of interest.

To validate predicted docking poses of **7i** and to provide more details on nature of SF_5 intermolecular interactions with D_3R and D_2R, we designed a multilevel QM/MM approach. The approach presented here combines a semiempirical level of theory (PM3) with more advanced and computationally demanding DFT calculations (M06-2X functional with def2-TZVP basis set).[59–61] PM3 calculations are inherently faster and can access tens to hundreds of picoseconds (ps) of dynamics. However, M06-2X level of theory has an advantage in implementing higher accuracy in dealing with intermolecular interactions. M06-2X functional has been shown through benchmarking studies to produce a good representation of noncovalent interactions.[59,62]

According to our results, poses of **7i** obtained through molecular docking remained stabilized during 100 ps of QM/MM simulations (Figure 3a,b). Compound **7i** was stabilized in D_2R and D_3R through an equilibrium between repulsive and attractive noncovalent interactions (NCIs) (Figure S6a,b). Comparing the initial docking poses and the ones obtained after QM/MM protocol, **7i** in D_3R slightly moved SF_5 moiety toward Pro362$^{7.31}$ residue and established interactions with it (Figures 3d and S7). This interaction was unseen through molecular

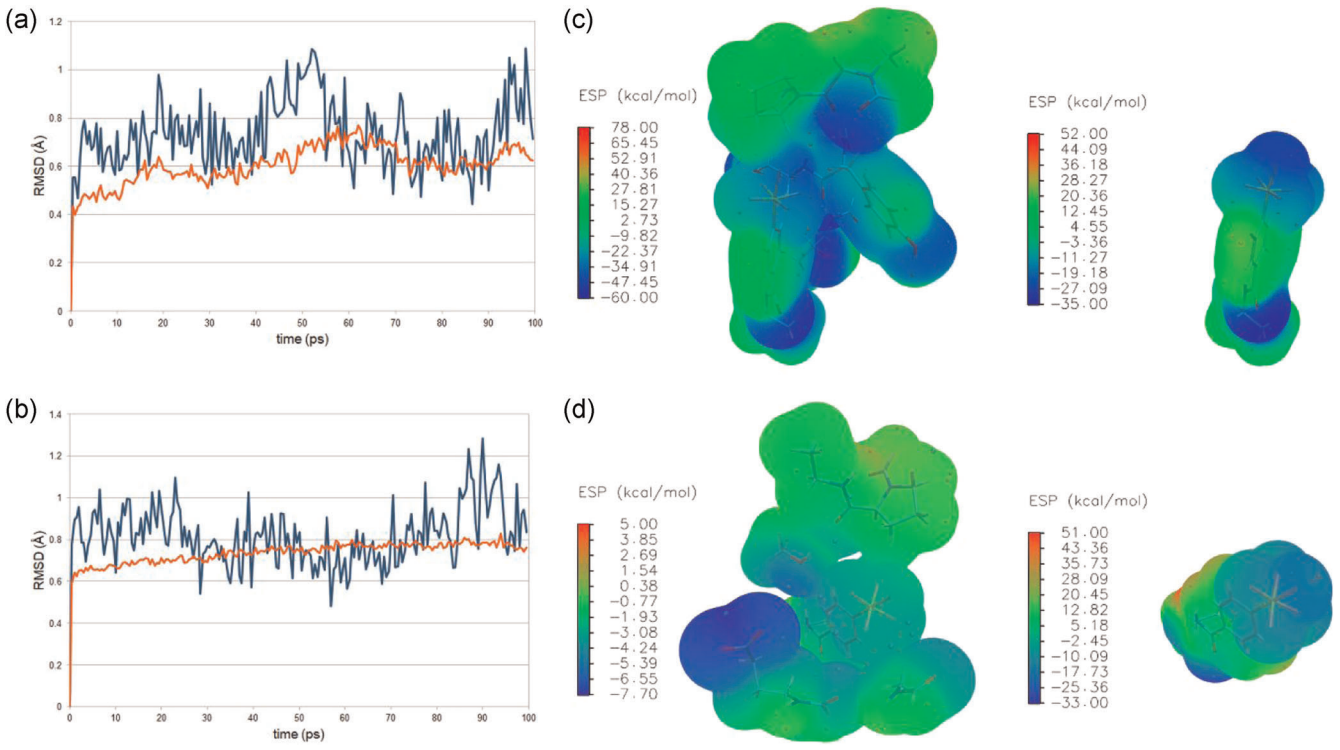

FIGURE 3 Root mean square deviation (RMSD) of atomic positions during 100 ps of QM/MM (quantum mechanics/molecular mechanics) (PM3) simulations, (a) D_2R:**7i** system and (b) D_3R:**7i** system and electrostatic potential (ESP) maps calculated on the M06-2X level of theory for the QM region after QM/MM minimizations, (c) D_2R:**7i** system and (d) D_3R:**7i** system, and after single-point calculations. The blue line in (a) and (b) indicates the RMSD calculated for the ligand atoms, whereas the red line represents the RMSD calculated for the protein backbone

docking. Contrary to the D_3R:**7i** complex, the D_2R:**7i** complex remained in a similar pose during the course of QM/MM simulation (Figure S7). However, the hydrogen bond between Ser409$^{7.35}$ of D_2R and fluorine of SF_5 moiety predicted by molecular docking (Figure 2b) disappeared after QM/MM, and it was replaced with C–H···F–S interaction (see below). After QM/MM simulations, we also may note that SF_5 moiety of **7i** was encircled with interacting D_3R residues, whereas upper fluorine of SF_5 was free and solvent-exposed. Contrary to this, SF_5 moiety of **7i** was buried in the sub-pocket of D_2R consisting of Tyr408$^{7.34}$, Pro405$^{7.31}$, and Ser409$^{7.35}$ (Figure 3c,d), which was in accordance with molecular docking results (Figure 2). Taken together, results indicate that molecular docking was reasonably accurate in predicting the pose of SF_5 moiety. Nevertheless, QM/MM protocol is indispensable in precise characterization of intermolecular interactions of SF_5.

Electrostatic potentials (ESP) were derived from electron densities and plotted on molecular van der Waals surfaces, to elucidate how protein environment affected electronic density in the ligand. ESP maps obtained after QM/MM calculations of QM regions of protein/ligand complexes (M06-2X level of theory) were compared with ESP maps obtained after single-point calculations of solo ligands in the same conformations (Figure 3c,d, cf. Supporting Information Materials). Results revealed that the protein environment affected the charge distribution of SF_5 moiety, indicating possible intramolecular interactions. Fluorine atoms closer to protein residues experienced more negative electrostatic potential, which could be explained with intramolecular interactions between SF_5 moiety and protein residues (Figure 3c,d).

To gain more details of specific spatial regions and the nature of interactions between proteins and SF_5 moiety of **7i**, NCI analysis was performed. Self-consistent field (SCF) densities for NCI analysis were obtained from QM/MM calculations on M06-2X level of theory. The NCI analysis indicated that all the intramolecular interactions between SF_5 moiety and D_2R/D_3R appear to be in the spectrum of delocalized weak interactions, $\mathrm{sign}(\lambda 2)\rho(r)$ between ± 0.01 a.u (Figure 4). No strong stabilizing interactions (e.g., hydrogen bonds) were detected. In the case of D_2R, C–H···F–S (Figure 4b,c) and S–F···C═O (Figure 4a) were the most prominent interactions (reduced density gradient, $s \leq 0.3$), whereas for the D_3R, C–H···F–S (Figure 4d) and S–F···O (Figure 4f) intermolecular interactions were observed as most important (reduced density gradient, $s \leq 0.3$). A recent empirical study on fluorine–protein interactions and ^{19}F NMR isotropic chemical shifts indicated that highly deshielded fluorines (also seen in SF_5 moiety) mainly participate in

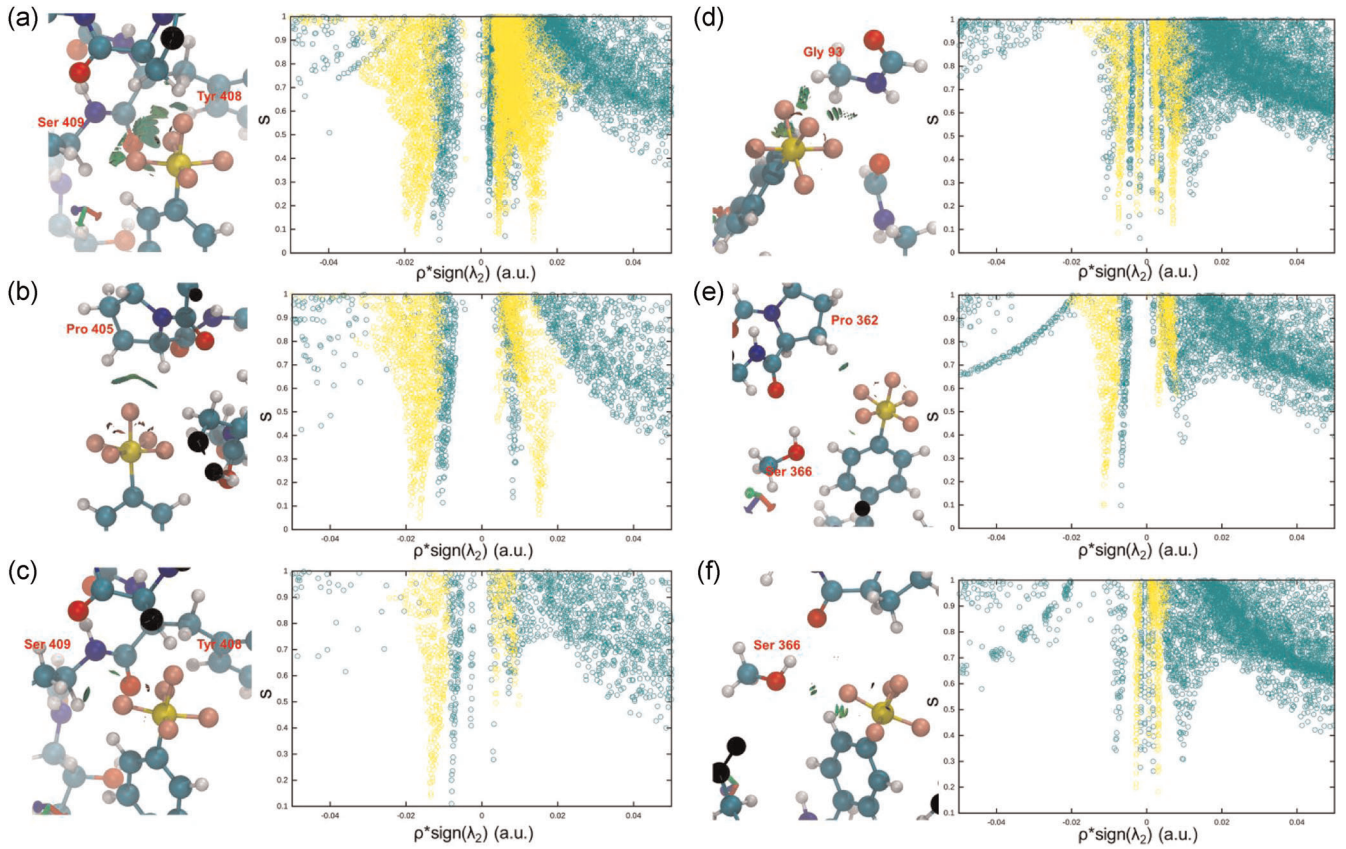

FIGURE 4 Results of the noncovalent interaction (NCI) analysis for D_2R:**7i** (a–c) and D_3R:**7i** (d–f) systems. On three-dimensional (3D) NCI plots, green isosurfaces represent delocalized weak attractive interactions (inter- and intramolecular), whereas red isosurfaces represent repulsive interactions calculated from self-consistent field (SCF) densities (quantum mechanics/molecular mechanics on M06-2× level of theory). On 2D NCI plots, $\mathrm{sign}(\lambda 2)\rho(r)$ versus reduced density gradient (s), green points represent results from SCF densities for intra- and intermolecular interactions, whereas yellow points represent results from promolecular densities only for intermolecular interactions. Due to inherent limitations of the NCI approach, it was not possible to omit intermolecular interactions from analysis for SCF densities

F···C=O orthogonal interactions with carbons from carbonyl groups and in interactions with aliphatic carbons, whereas F···O interaction was detected but classified as less common for deshielded fluorines.[63] Our results are in agreement with these empirical findings.

Furthermore, we evaluated a promolecular approach in characterizing NCIs of SF_5. The promolecular method (compared with SCF approach) has an advantage in much faster calculations allowing us to analyze interactions between the whole ligand and all interacting residues (not limited only to the SF_5 moiety). Comparative 2D NCI plots (Figure 4) indicated that specific intramolecular interactions obtained through SCF calculations are mainly positioned on similar values of electron density and have similar values of reduced density gradients as for promolecular NCI calculations. 3D NCI plots indicated that promolecular approach successfully reproduced the spatial position of the interactions (Figures 4 and S6). However, in the case of the **7i**:D_2R complex, the promolecular method predicted the existence of stronger interactions (higher values of electron density) in some cases (Figure 4a,b). After visual inspection of 3D and 2D NCI plots, we concluded that the promolecular approach could be a viable and faster alternative in the analysis of noncovalent interactions between SF_5 moiety and D_2R and D_3R, but some caveats regarding bond strengths should be considered.

Finally, the promolecular method was used to access whole intermolecular interactions between **7i** and D_2R/D_3R (Figure S6). Considering results from both approaches (promolecular and SCF), we may conclude that (pentafluorosulfanyl)phenyl moiety of **7i** achieved a larger number of interactions with D_2R through SF_5 moiety (Figure 4), whereas its interaction with D_3R was driven mainly through phenyl moiety (Figure S6). This is in accordance with the results of molecular docking where steric effects of –p SF_5 moiety of **7i** prevented interaction with Tyr $408^{7.34}$ in D_2R (see above). In addition, convergence of QM/MM (PM3) simulations was accessed by integrating promolecular densities for each frame. Results indicated well-converged simulations (Figure S6).

3 | CONCLUSION

All of the 10 synthesized compounds exhibited nanomolar affinities at dopamine D_2R and D_3R. Most of them expressed a slight preference for D_3R. Compound **7c** showed the highest affinity at D_2R, pK_i (D_2R) = 8.02, and **7i** showed the highest affinity at D_3R, pK_i (D_3R) = 8.42. Our studies on the structure–activity relationship have determined that the prerequisite for the best affinity toward receptors of interest is the four methylene group linker between the amide and the aryl moiety (**7c**) pK_i (D_2R) = 8.02; pK_i (D_3R) = 8.25. The compound containing five-methylene group linker (**7d**), pK_i (D_2R) = 7.87 pK_i (D_3R) = 7.51, displayed a higher affinity when compared to the compounds that contain three-methylene (**7b**), pK_i (D_2R) = 6.82 pK_i (D_3R) = 6.90, or two-methylene linker (**7a**), pK_i (D_2R) = 6.98; pK_i (D_3R) = 6.74. Further optimization was, therefore, performed with four-methylene linkers. In vitro data confirmed that the substitution of benzene ring with the coumarin moiety (**7e**, **7f**) resulted in remaining affinity to both D_2R and D_3R, whereas substitution with the 6-methoxy group at coumarin moiety (**7f**) resulted in increased affinities to both D_2R and D_3R. Compound **7i** that contains the novel SF_5 moiety showed not only the highest affinity at D_3R, but also the highest selectivity (SI = 20.5). Introduction of the SF_5 moiety (**7i**) into the *para*-position of the western part of the molecule led to increased selectivity, more than 10-fold, toward D_3R. When the eastern part was changed to 4-(2,3-dichlorophenyl)piperazino substituents (**7j**), the selectivity was reduced in comparison to **7i**, but was still more than threefold toward D_3R (when compared to the parent compound [**7c**]). If the position of SF_5 group was changed, from *para*- to *meta*-position, with both groups in the eastern part (2-methoxy and 2,3-dichloro) (**7g**, **7h**) high affinities were obtained at D_3R, pK_i (D_3R) = 8.30 and pK_i (D_3R) = 8.03, respectively, with about sixfold increase in selectivity when compared with that of the parent molecule **7c**.

Our in silico results have confirmed that the protonated phenylpiperazine moiety binds to OBS at both D_2R and D_3R, forming a crucially important salt bridge between positively charged nitrogen on piperazine and Asp110 $^{3.32}$. The arylamide moiety binds to SBP at D_3R and EBP at D_2R, which correlates with previously reported results. The compound with the highest affinity and selectivity toward D_3R (**7i**) was particularly challenging due to the new SF_5 moiety that is neither synthetically nor computationally fully characterized. To the best of the authors' knowledge, for the first time, the QM/MM approach was used to access intermolecular interactions of SF_5 with biomacromolecule. The QM/MM approach revealed that the protein environment changed electron density distribution in SF_5 moiety, whereas the NCI analysis confirmed that all of intramolecular interactions between SF_5 moiety and receptors of interest are in the class of week delocalized interactions. In addition, it has been shown that *m*-substituted SF_5 derivative was optimal for interaction with the binding site of D_2R, whereas *p*-substitution with this moiety led to decreased affinity at D_2R due to steric hindrance, which is in accordance with in vitro results obtained.

On the basis of reported results, we conclude that all of the 10 synthesized compounds represent potent, novel pharmacological tools in the treatment of various neurological diseases. Compound **7i** that contains a pentafluorosulfanyl moiety has shown the highest in vitro affinity and interesting binding mode toward receptors of interest in this small series. The SF_5 group can be taken as a promising substituent in dopamine GPCR ligands, and therefore will be further investigated in other compound classes of aminergic GPCRs.

4 | EXPERIMENTAL

4.1 | Chemistry

4.1.1 | General

All starting materials were obtained from Sigma Aldrich and Apollo Scientific and used without further purification. Analytical thin-layer

chromatography was carried out on precoated TLC sheets ALUGRAM® Xtra SIL G/UV254 (Macherey-Nagel) with visualization under UV light. Mass spectra have been determined using Advion Mass Express. Atmospheric-pressure chemical ionization (APCI) was used as a method of ionization, operating in positive mode. Data are shown as $[M+H^+]^+$. Melting points (mps) were determined by Büchi Schmelzpunkt M-565 (Büchi) with an open capillary tube and were uncorrected. ^1H and ^{13}C NMR spectra of compounds of interest were measured at Bruker Avance-III 300 (2010) and Bruker Avance-III 600 (2011). Deuterated dimethyl sulfoxide (DMSO-d_6) was used as a solvent for NMR and tetramethylsilane was used as a standard. Chemical shifts are given as parts per million (ppm) and reported as follows: s (singlet), d (doublet), dd (double of doublets), t (triplet), q (quartet), p (pentet), or m (multiplet). The coupling constant (*J*) is given in Hertz (Hz). Purification of compounds has been accomplished using flash chromatography: Biotage Isolera™ Spektra Systems with ACI™ and Assist (Biotage). SNAP KP-Sil and SNAP KP-Sil ULTRA (Biotage) were used as stationary phase and dichloromethane (DCM) and MeOH were used as mobile phase. Solvents have been evaporated using a Rotavapor R II (Büchi) with a PC 3001 VARIO Chemie-Vacuum pump (Vacuubrand) and CVC 3000 Vacuum controlling system. The compounds have been dried with the high-vacuum pump (Hybrid-Pumpe RC 6; Vacuubrand). Compound purities were determined by an elementary analysis Vario MICRO cube elemental analyzer (Elementar Analysensysteme) and liquid chromatography-mass spectrometry (LC-MS): Elute SP (HPG 700) Bruker Daltronicsand amaZon^{speed} ion trap LC/MSn system (ESI-MS). Method: Alternating ion polarity: on; scan range: *m/z*: 80–1200; nebulizer: nitrogen, 15 Psi; dry gas: nitrogen, 8 l/min, 200°C; mass range mode: UltraScan; column: Intensity Solo 2 C18 (100 × 2.1 mm); temperature: 50°C; mobile phase: A: water hypergrade for LC-MS with 0.1% formic acid (v/v) (Merck); B: acetonitrile hypergrade for LC-MS (for LC-MS); method of analysis: 0–4-min 98% A, 4–5 min gradient 95% A, 5–9 min 95% A, 9–16 min gradient 5% A, 16–17 min gradient to 0% A, reconditioning: 17–18 min gradient to 98% A, 18–21 min 98% A (see Supporting Information Materials).

The InChI codes of the investigated compounds, together with some biological activity data, are provided as Supporting Information.

4.1.2 | General procedure for the synthesis of *N*-{ω-[4-(2-methoxyphenyl)piperazin-1-y]alkyl}-phthalimides (4a–c)

To a stirred solution of suitable *N*-(ω-bromo-alkyl)phthalimides **2a**–**c** (1.2 eq.) in acetone, 1-(2-methoxyphenyl)piperazine (**1a**) (1 eq) and anhydrous K_2CO_3 (6–12 eq.) were added. The reaction mixture was stirred at reflux temperature overnight. After cooling down the reaction mixture to room temperature, inorganic salts were filtered off and the filtrate was concentrated to dryness. The crude reaction mixture was partitioned between EtOAc and water. The organic layer was separated and the remaining aqueous layer was extracted with EtOAc (3×) and washed with brine. The combined organic layers were dried over anhydrous $MgSO_4$, filtered and concentrated under reduced pressure. The crude mixture was purified by flash column chromatography (sorbent: SiO_2, eluent: DCM/MeOH gradient: 100–95%/0–5%) to obtain **4a**–**c**.

*2-{2-[4-(2-Methoxyphenyl)piperazin-1-yl]ethyl}isoindoline-1,3-dione (**4a**)*[64,65]

Yellow solid. Yield: 42%. ^1H NMR (300 MHz, DMSO-d_6) δ 7.93–7.81 (m, 4H), 6.97–6.79 (m, 4H), 3.75 (s, 3H), 3.72 (t, *J* = 6.5 Hz, 2H), 2.88–3.0 (m, 4H), and 2.62–2.52 (m, 6H). MS (APCI[+]): *m/z* $[M+H^+]^+$: calculated for $[C_{12}H_{24}N_3O_3]^+$: 366.2, found: 366.1.

*2-{3-[4-(2-Methoxyphenyl)piperazin-1-yl]propyll}isoindoline-1,3-dione (**4b**)*[66]

Yellow solid. Yield: 51%. ^1H NMR (300 MHz, DMSO-d_6) δ 7.93–7.77 (m, 4H), 6.96–6.75 (m, 3H), 6.68 (dd, *J* = 7.6, 1.5 Hz, 1H), 3.72 (s, 3H), 3.67 (t, *J* = 6.7 Hz, 2H), 2.75–2.62 (m, 4H), 2.44–2.33 (m, 6H), and 1.77 (p, *J* = 6.6 Hz, 2H). MS (APCI[+]) *m/z* $[M+H^+]^+$: calculated for $[C_{22}H_{26}N_3O_3]^+$: 380.1, found: 380.3.

*2-{4-[4-(2-Methoxyphenyl)piperazin-1-yl]butyl}isoindoline-1,3-dione (**4c**)*[64,66]

Yellow solid. Yield: 96%. ^1H NMR (300 MHz, DMSO-d_6) δ 7.93–7.78 (m, 4H), 6.99–6.79 (m, 4H), 3.75 (s, 3H), 3.59 (t, *J* = 6.9 Hz, 2H), 2.97–2.87 (m, 4H), 2.48–2.41 (m, 4H), 2.32 (t, *J* = 7.2 Hz, 2H), 1.61 (p, 2H), and 1.45 (p, *J* = 7.3 Hz, 2H). MS (APCI[+]) *m/z* $[M+H^+]$: calculated for $[C_{23}H_{28}N_3O_3]^+$: 394.2, found: 394.2.

4.1.3 | General procedure for the synthesis of ω-[4-(2-methoxyphenyl)piperazin-1-yl]alkylamines (6a–c): Route I

To a stirred solution of *N*-{ω-[4-(2-methoxyphenyl)piperazin-1-yl]alkyl}phthalimide **4a** (0.76 mmol), **4b** (2.24 mmol), and **4c** (2.82 mmol) in 30 ml of MeOH, 0.5 ml of hydrazine monohydrate (64–65% aq. solution) was added and stirred upon reflux for 2 h. After 2 h, 5 ml of 2 M HCl was added to the hot solution and the reaction mixture was stirred at reflux temperature for another hour. After cooling down to room temperature, the reaction mixture was filtered, and the filtrate was concentrated to dryness. Then, 20 ml of 2 M NaOH was added to the concentrated filtrate and residues were washed with water. Extraction was performed with EtOAc and water. The organic layer was separated and the remaining aqueous layer was extracted with EtOAc (3×) and washed with brine. The combined organic layers were dried with anhydrous $MgSO_4$, filtered and concentrated under reduced pressure. Crude products were purified by flash column chromatography (sorbent: SiO_2, eluent: DCM/MeOH/NH_3).

*2-[4-(2-Methoxyphenyl)piperazin-1-yl]ethanamine (**6a**)*[64,65,67]

Yellow oil. Yield: 46%. ^1H NMR (300 MHz, DMSO-d_6) δ 7.03–6.76 (m, 4H), 3.76 (s, 3H), 3.02–2.89 (br s, 4H), 2.74 (d, *J* = 6.7 Hz, 2H), 2.46–2.35 (m, 2H), and 1.81–1.73 (m, 6H). MS (APCI[+]) *m/z* $[M+H^+]^+$: calculated for $[C_{13}H_{22}N_3O]^+$: 236.2, found: 236.4.

*3-[4-(2-Methoxyphenyl)piperazin-1-yl]propanamine (**6b**)*[65]

Yellow oil. Yield: 35%. ^{1}H NMR (300 MHz, DMSO-d_6) 7.12–6.78 (m, 4H), 3.76 (s, 3H), 2.95–3.00 (br s, 4H), 2.84–2.75 (m, 2H), 2.42–2.32 (m, 2H), and 2.01–1.60 (m, 8H). MS (APCI[+]) *m/z* [M+H$^+$]$^+$: calculated for $[C_{14}H_{24}N_3O]^+$: 250.2, found: 250.4.

*4-[4-(2-Methoxyphenyl)piperazin-1-yl]butanamine (**6c**)*[65–68]

Yellow oil. Yield: 69%. ^{1}H NMR (300 MHz, DMSO-d_6) δ 7.10–6.74 (m, 4H), 3.75 (d, *J* = 3.0 Hz, 3H), 2.94 (t, *J* = 4.6 Hz, 4H), 2.61–2.53 (m, 2H), 2.40–2.46 (m, 6H), 2.29 (t, *J* = 6.9 Hz, 2H), and 1.55–1.29 (m, 4H). MS (APCI[+]) *m/z* [M+H$^+$]$^+$: calculated for $[C_{15}H_{26}N_3O]^+$: 264.2, found: 264.1.

4.1.4 | General procedure for the synthesis of ω-[4-(2-methoxyphenyl)piperazinyl]alkylnitriles and ω-[4-(2,3-dichlorophenyl)piperazin-1-yl]alkylnitriles (5a–c)

To a stirred solution of 1-(2-methoxyphenyl)piperazine (1 eq.) (**1a**) or 1-(2,3-dichlorophenyl)piperazine (**1b**) (1.1 eq.) in acetone, corresponding bromo-alkyl-nitriles **3a** (6.76 mmol, 1 eq.) and **3b** (6.17 mmol, 1 eq.), and anhydrous K_2CO_3 (6–12 eq.) were added. The reaction mixture was heated up to reflux for 16 h. After cooling down, the inorganic salts were filtered off and the filtrate was concentrated to dryness. The crude product was partitioned between EtOAc (3×) and water. The organic layer was washed with a saturated solution of $NaHCO_3$ and brine and dried over anhydrous $MgSO_4$. Crude products were purified using flash column chromatography (sorbent: SiO_2, eluent: DCM/MeOH gradient:100–95%/0–5%).

*4-[4-(2-Methoxyphenyl)piperazin-1-yl]butannitrile (**5a**)*[67,68]

Yellow solid. Yield: 69%. ^{1}H NMR (300 MHz, DMSO-d_6) δ 7.00–6.85 (m, 4H), 3.78 (s, 3H), 2.97–3.02 (br s, 4H), 2.47–2.50 (m, 6H), 2.41 (t, *J* = 6.9 Hz, 2H), and 1.76 (p, *J* = 7.0 Hz, 2H). MS (APCI[+]) *m/z* [M+H$^+$]$^+$: calculated for $[C_{15}H_{22}N_3O]^+$: 260.2 and 261.2, found: 260.4 and 261.4.

*4-[4-(2,3-Dichlorophenyl)piperazin-1-yl]butannitrile (**5b**)*[68]

Yellow solid. Yield: 95%. ^{1}H NMR (300 MHz, DMSO-d_6) δ 7.34–7.27 (m, 2H), 7.14 (dd, *J* = 6.2, 3.5 Hz, 1H), 3.04–2.91 (br s, 4H), 2.57–2.52 (m, 4H), 2.50–2.51 (m, 2H) 2.42 (t, *J* = 6.8 Hz, 2H), and 1.75 (p, *J* = 6.9 Hz, 2H). MS (APCI[+]) *m/z* [M+H$^+$]$^+$: calculated for $[C_{14}H_{18}Cl_2N_3]^+$: 298.1 and 300.1, found: 299.0 and 300.0.

*5-[4-(2-Methoxyphenyl)piperazin-1-yl]pentannitrile (**5c**)*[69,70]

Transparent oil. Yield: 88%. ^{1}H NMR (300 MHz, DMSO-d_6) δ 7.05–6.80 (m, 4H), 3.77 (s, 3H), 3.00–2.91 (br s, 4H), 2.56–2.52 (m, 2H), 2.46–2.50 (m, 4H), 2.34 (t, *J* = 6.5 Hz, 2H), and 1.70–1.47 (m, 4H). MS (APCI[+]) *m/z* [M+H$^+$]$^+$: calculated for $[C_{16}H_{24}N_3O]^+$: 274.2 and 275.2, found: 274.1 and 275.1.

4.1.5 | General procedure for the synthesis of ω-[4-(2-methoxyphenyl)-piperazinyl]alkylamines and ω-[4-(2,3-dichlorophenyl)-piperazinyl]alkylamines (6c–e): Route II

Obtained nitriles **5a** (3.35 mmol), **5b** (4.05 mmol), and **5c** (5.10 mmol) were dissolved in 50 ml ammonia solution in methanol and consequently subjected to catalytic hydrogenation using freshly prepared Raney nickel (from 500 mg of aluminum nickel alloy, as previously described).[71] The reaction mixture was reduced with H_2 at 5 bar pressure overnight. The reaction mixture was filtered off through celite and the filtrate was evaporated to dryness. The obtained amines were used without further purification into the next reaction step.

*4-[4-(2-Methoxyphenyl)piperazin-1-yl]butan-1-amine (**6c**)*[68,72]

Yellow oil. Yield: 85%. ^{1}H NMR (300 MHz, DMSO-d_6) δ 6.97–6.83 (m, 4H), 3.77 (s, 3H), 3.01–2.87 (br s, 4H), 2.61–2.53 (m, 2H), 2.44–2.52 (m, 6H), 2.30 (t, *J* = 7.2 Hz, 2H), and 1.53–1.30 (m, 4H). MS (APCI[+]) *m/z* [M+H$^+$]$^+$: calculated for $[C_{15}H_{26}N_3O]^+$: 264.2, found: 265.2.

*4-[4-(2,3-Dichlorophenyl)piperazin-1-yl]butan-1-amine (**6d**)*[68]

Light yellow solid. Yield: 59%. ^{1}H NMR (300 MHz, DMSO-d_6) δ 7.34–7.24 (m, 2H), 7.13 (dd, *J* = 6.3, 3.3 Hz, 1H), 3.02–2.92 (br s, 4H), 2.62–2.51 (m, 4H), 2.45–2.47 (m, 4H), 2.31 (t, *J* = 7.1 Hz, 2H), and 1.55–1.28 (m, 4H). MS (APCI[+]) *m/z* [M+H$^+$]$^+$: calculated for $[C_{14}H_{22}Cl_2N_3]^+$: 302.1 and 304.1, found: 302.4 and 304.4.

*5-[4-(2-Methoxyphenyl)piperazin-1-yl]pentan-1-amine (**6e**)*[69]

Yellow oil. Yield: 79%. ^{1}H NMR (300 MHz, DMSO-d_6) δ 7.03–6.79 (m, 4H), 3.76 (s, 3H), 3.07–2.85 (br s, 4H), 2.58–2.52 (m, 2H), 2.40–2.46 (m, 4H), 2.29 (t, *J* = 8.0, 6.5 Hz, 2H), and 1.52–1.20 (m, 6H). MS (APCI[+]) *m/z* [M+H$^+$]$^+$: calculated for $[C_{16}H_{28}N_3O]^+$: 278.2, found: 278.5.

4.1.6 | General procedure for amide synthesis (7a–j)

To a stirred solution of **6a**–**e** (1 eq.) and corresponding acid (1.1 eq.) in DCM, HOBt (1.1 eq.) and EDC (1.1 eq.) were added. The reaction mixture was stirred at room temperature overnight. Into the reaction mixture, saturated solution of $NaHCO_3$ was added for quenching and it was stirred for 15 min. The crude product was partitioned between DCM (3×) and water. The combined organic layers were washed with a saturated solution of $NaHCO_3$ and brine, dried over anhydrous $MgSO_4$, filtered, and concentrated under reduced pressure. The crude mixtures were purified by flash column chromatography (sorbent: SiO_2, eluent: DCM/MeOH gradient: 100–90%/0–10%).

*3-Bromo-4-methoxy-*N*-{2-[4-(2-methoxyphenyl)piperazin-1-yl]-ethyl})benzamide (**7a**)*

Light yellow solid. Yield: 22%. ^{1}H NMR (300 MHz, DMSO-d_6) δ 8.42 (t, *J* = 5.6 Hz, 1H), 8.09 (d, *J* = 2.2 Hz, 1H), 7.88 (dd, *J* = 8.6, 2.2 Hz, 1H),

7.19 (d, J = 8.7 Hz, 1H), 6.97–6.82 (m, 4H), 3.90 (s, 3H), 3.77 (s, 3H), 3.40 (t, J = 6.5 Hz, 2H), 3.02–2.88 (br s, 4H), and 2.63–2.54 (m, 4H). ^{13}C NMR (75 MHz, DMSO-d_6) δ 164.28, 157.47, 151.93, 141.21, 131.75, 128.41, 127.95, 122.31, 120.79, 117.85, 112.07, 111.86, 110.23, 57.01, 56.48, 55.27, 53.01, 50.01, and 36.86. Elemental analysis (calculated/found): %C 56.26/55.75, %H 5.85/5.87, and %N 9.37/9.50; mp = 163.4°C; R_f = 0.30 (eluent: DCM/MeOH 95:5). MS (APCI[+]) m/z $[M+H^+]^+$: calculated for. $[C_{21}H_{27}BrN_3O_3]^+$: 448.1; 450.1; and 449.1, found: 449.0; 450.0; and 451.0.

*3-Bromo-4-methoxy-*N*-{(3-[4-(2-methoxyphenyl)piperazin-1-yl]-propyl}benzamide (**7b**)*

White solid. Yield: 30%. ^{1}H NMR (300 MHz, DMSO-d_6) δ 8.49 (t, J = 5.5 Hz, 1H), 8.08 (d, J = 2.2 Hz, 1H), 7.88 (dd, J = 8.6, 2.2 Hz, 1H), 7.18 (d, J = 8.7 Hz, 1H), 6.99–6.81 (m, 4H), 3.90 (s, 3H), 3.76 (s, 3H), 3.32–3.24 (br s, 2H), 3.00–2.90 (m, 4H), 2.50–2.60 (m, 4H), 2.38 (t, J = 7.0 Hz, 2H), and 1.70 (p, J = 7.0 Hz, 2H). ^{13}C NMR (75 MHz, DMSO-d_6) δ 164.25, 157.42, 151.93, 141.21, 131.67, 128.41, 128.05, 122.30, 120.79, 117.86, 112.04, 111.86, 110.21, 56.47, 55.79, 55.27, 53.02, 50.04, 37.96, and 26.14. Elemental analysis (calculated/found): %C 57.15/56.70, %H 6.10/6.06, and %N 9.09/8.82; mp = 127.6°C; R_f = 0.33 (eluent: DCM/MeOH 95:5). MS-(APCI[+]) m/z $[M+H^+]^+$: calculated for $[C_{22}H_{29}BrN_3O_3]^+$: 462.1 and 464.1, found: 462.1 and 464.1.

*3-Bromo-4-methoxy-*N*-{4-[4-(2-methoxyphenyl)piperazin-1-yl]-butyl}benzamide (**7c**)*

White solid. Yield: 44%. ^{1}H NMR (300 MHz, DMSO-d_6) δ 8.43 (t, J = 5.6 Hz, 1H), 8.09 (d, J = 2.2 Hz, 1H), 7.88 (dd, J = 8.6, 2.2 Hz, 1H), 7.18 (d, J = 8.7 Hz, 1H), 6.96–6.83 (m, 4H), 3.90 (s, 3H), 3.76 (s, 3H), 3.26 (q, J = 6.3 Hz, 2H), 3.00–2.86 (br s, 4H), 2.45–2.50 (m, 4H), 2.33 (t, J = 6.7 Hz, 2H), and 1.60–1.43 (m, 4H). ^{13}C NMR (75 MHz, DMSO-d_6) δ 164.21, 157.40, 151.93, 141.26, 131.72, 128.40, 128.08, 122.27, 120.79, 117.82, 112.03, 111.87, 110.20, 57.60, 56.46, 55.27, 53.01, 50.04, 27.04, and 23.80. Elemental analysis (calculated/found): %C 57.99/57.83, %H 6.35/6.38, and %N 8.82/8.68; mp = 162.0°C; R_f = 0.37 (eluent: DCM/MeOH 95:5). MS (APCI[+]) m/z $[M+H^+]^+$: calculated $[C_{23}H_{31}BrN_3O_3]^+$: 476.1; 477.1; and 478.1, found: 476.0; 477.0; and 478.0.

*3-Bromo-4-methoxy-*N*-{5-[4-(2-methoxyphenyl)piperazin-1-yl]-pentyl}benzamide (**7d**)*

White solid. Yield: 30%. ^{1}H NMR (600 MHz, DMSO-d_6) δ 8.42 (t, J = 5.6 Hz, 1H), 8.09 (d, J = 2.2 Hz, 1H), 7.88 (dd, J = 8.6, 2.2 Hz, 1H), 7.18 (d, J = 8.7 Hz, 1H), 6.96–6.80 (m, 4H), 3.90 (s, 3H), 3.76 (s, 3H), 3.24 (q, J = 6.6 Hz, 2H), 3.00–2.87 (br s, 4H), 2.45–2.50 (m, 4H), 2.32 (s, 2H), 1.58–1.44 (m, 4H), and 1.36–1.27 (m, 2H). ^{13}C NMR (150 MHz, DMSO-d_6) δ 164.68, 157.91, 152.43, 141.73, 132.22, 128.91, 128.59, 122.79, 121.29, 118.32, 112.52, 112.37, 110.71, 58.27, 56.97, 55.77, 53.49, 50.47, 40.54, 29.42, 26.39, and 24.81. LC-MS (ESI[+]) = 95.08; mp = 110.7°C; R_f = 0.4 (eluent DCM/MeOH 9:1). MS (APCI[+]) m/z $[M+H^+]^+$: calculated for $[C_{24}H_{33}BrN_3O_3]^+$: 490.2 and 492.2, found: 490.2 and 492.1.

N*-{4-[4-(2-Methoxyphenyl)piperazin-1-yl]butyl}-2-oxo-2*H*-chromene-3-carboxamide (**7e**)[66,73]*

Yellow powder. Yield: 39%. ^{1}H NMR (300 MHz, DMSO-d_6) δ 8.85 (s, 1H), 8.69 (t, J = 5.8 Hz, 1H), 7.99 (dd, J = 7.8, 1.6 Hz, 1H), 7.75 (td, J = 8.7, 7.3, 1.7 Hz, 1H), 7.54–7.39 (m, 2H), 6.97–6.79 (m, 4H), 3.76 (s, 3H), 3.35–3.40 (q, 2H), 2.99–2.89 (br s, 4H), 2.45–2.50 (m, 4H), 2.35 (t, J = 6.7 Hz, 2H), and 1.62–1.38 (m, 4H). ^{13}C NMR (75 MHz, DMSO-d_6) δ 161.01, 160.38, 153.81, 151.93, 147.19, 141.25, 133.97, 130.18, 125.09, 122.28, 120.79, 119.20, 118.47, 117.83, 116.10, 111.87, 57.50, 55.27, 52.99, 50.03, 26.95, and 23.65. LC-MS (ESI[+]) = 97.14%; mp = 122.5°C; R_f = 0.28 (eluent DCM/MeOH 95:5). MS (APCI[+]) m/z $[M+H^+]^+$: calculated for $[C_{25}H_{30}N_3O_4]^+$: 436.2 and 437.2, found: 436.1 and 437.1.

*6-Methoxy-*N*-{4-[4-(2-methoxyphenyl)piperazin-1-yl]butyl}-2-oxo-2*H*-chromene-3-carboxamide (**7f**)*

Light orange solid. Yield: 67%. ^{1}H NMR (300 MHz, DMSO-d_6) δ 8.82 (s, 1H), 8.73 (t, J = 5.7 Hz, 1H), 7.56 (d, J = 3.0 Hz, 1H), 7.46 (d, J = 9.1 Hz, 1H), 7.34 (dd, J = 9.1, 3.0 Hz, 1H), 6.99–6.81 (m, 4H), 3.82 (s, 3H), 3.76 (s, 3H), 3.36 (s, 2H), 2.95 (br s, 4H), 2.51 (m, 4H), 2.36 (s, 2H), and 1.54 (s, 4H). ^{13}C NMR (75 MHz, DMSO-d_6) δ 161.03, 160.53, 155.92, 151.93, 148.31, 147.11, 128.11,122.30, 121.86, 120.79, 119.24, 117.84, 117.23, 117.05, 111.86, 111.79, 56.65, 55.82, 55.25, 52.95, 49.98, 40.54, 26.90, and 23.60. Elemental analysis (calculated/found): %C 67.08/66.81, %H 6.71/6.67, and %N 9.03/8.90; mp = 140.4°C; R_f = 0.31 (eluent DCM/MeOH 95:5). MS-((APCI[+]): m/z $[M+H^+]^+$: calculated for $[C_{26}H_{32}N_3O_5]^+$: 466.2 and 467.2, found: 466.3 and 467.1.

N*-{4-[4-(2-Methoxyphenyl)piperazin-1-yl]butyl}-3-(pentafluoro-λ6-sulfanyl)benzamide (**7g**)*

White solid. Yield: 42%. ^{1}H NMR (300 MHz, DMSO-d_6) δ 8.82 (t, J = 5.6 Hz, 1H), 8.32 (t, J = 1.9 Hz, 1H), 8.19–8.02 (m, 2H), 7.73 (t, J = 8.0 Hz, 1H), 6.99–6.83 (m, 4H), 3.76 (s, 3H), 3.33–3.28 (m, 2H), 3.02–2.88 (br s, 4H), 2.52–2.60 (m, 4H), 2.38 (t, J = 6.8 Hz, 2H), and 1.64–1.45 (m, 4H). ^{13}C NMR (75 MHz, DMSO-d_6) δ 164.01, 152.78, 151.92, 141.16, 135.66, 131.06, 129.77, 128.21, 124.28, 122.33, 120.79, 117.82, 111.86, 57.44, 55.25, 52.92, 49.89, 26.86, and 23.64. Elemental analysis (calculated/found): %C 53.54/53.24, %H 5.72/5.87, %N 8.51/8.25, and %S 6.50/6.24; mp = 123.2°C; R_f = 0.49 (eluent DCM/MeOH 9:1). MS (APCI[+]) m/z $[M+H^+]^+$: calculated for $[C_{22}H_{29}F_5N_3O_2S]^+$: 494.2, found: 494.9.

N*-{4-[4-(2,3-Dichlorophenyl)piperazin-1-yl]butyl}-3-(pentafluoro-λ6-sulfanyl)benzamide (**7h**)*

Beige solid. Yield: 39%. ^{1}H NMR (300 MHz, DMSO-d_6) δ 8.80 (t, J = 5.3 Hz, 1H), 8.31 (d, J = 2.1 Hz, 1H), 8.22–8.02 (m, 2H), 7.72 (t, J = 8.0 Hz, 1H), 7.34–7.24 (m, 2H), 7.17– 7.06 (m, 1H), 3.30 (t, J = 5.9 Hz, 2H), 3.06–2.89 (br s, 4H), 2.51–2.55 (m, 4H), 2.36 (t, J = 6.7 Hz, 2H), and 1.68–1.41 (m, 4H). ^{13}C NMR (75 MHz, DMSO-d_6) δ 164.01, 153.1, 151.18, 135.67, 132.58, 131.06, 129.77, 128.38, 128.21, 125.96, 124.50, 124.29, 119.45, 57.39, 52.77, 50.91, 40.03, 26.88, and 23.75. LC-MS (ESI[+]) = 95.63%; mp = 104.8°C; R_f = 0.33 (eluent: DCM/MeOH 95:5). MS (APCI[+]) m/z $[M+H^+]^+$: calculated for $[C_{21}H_{25}Cl_2F_5N_3OS]^+$: 532.1; 533.1; and 534.1, found: 532,1; 533.1; and 534.1.

*N-{4-[4-(2-Methoxyphenyl)piperazin-1-yl]butyl}-4-(pentafluoro-λ6-sulfanyl)benzamide (**7i**)*

White solid. Yield: 46%. ^{1}H NMR (300 MHz, DMSO-d_6) δ 8.74 (t, J = 5.7 Hz, 1H), 8.02 (s, 4H), 6.95–6.83 (m, 4H), 3.76 (s, 3H), 3.29 (t, J = 6.4, 5.1 Hz, 2H), 3.01–2.88 (br s, 4H), 2.45–2.50 (m, 4H), 2.35 (d, J = 8.5 Hz, 2H), and 1.64–1.45 (m, 4H). ^{13}C NMR (75 MHz, DMSO-d_6) δ 164.43, 151.93, 141.24, 138.17, 128.27, 125.94, 122.28, 120.79, 117.82, 111.87, 57.55, 55.27, 52.99, 50.02, 40.03, 26.90, and 23.74. Elemental analysis (calculated/found): %C 53.54/53.50, %H 5.72/5.68, %N 8.51/8.38, and %S 6.50/6.34; mp = 137.7°C; R_f = 0.5 (eluent: DCM/MeOH 9:1). MS (APCI[+]) m/z $[M+H^+]^+$: calculated for $[C_{22}H_{29}F_5N_3O_2S]^+$: 494.2, found: 494.9.

*N-{4-[4-(2,3-Dichlorophenyl)piperazin-1-yl]butyl}-4-(pentafluoro-λ6-sulfanyl)benzamide (**7j**)*

White solid. Yield: 39%. ^{1}H NMR (300 MHz, DMSO-d_6) δ 8.73 (t, J = 5.4 Hz, 1H), 8.02 (s, 4H), 7.36–7.25 (m, 2H), 7.13 (dd, J = 6.0, 3.6 Hz, 1H), 3.29 (t, 2H), 3.04–2.92 (br s, 4H), 2.50–2.60 (m, 4H), 2.37 (t, J = 6.7 Hz, 2H), and 1.63–1.44 (m, 4H). ^{13}C NMR (150 MHz, DMSO-d_6) δ 164.01, 151.18, 135.67, 132.58, 131.06, 129.77, 128.38, 125.96, 124.29, 119.45, 57.39, 52.77, 50.91, 26.88, and 23.75. LC-MS (ESI[+]) = 96.80%; mp = 129.0°C; R_f = 0.33 (eluent: DCM/MeOH 95:5). MS (APCI[+]) m/z $[M+H^+]^+$: calculated for $[C_{21}H_{25}Cl_2F_5N_3OS]^+$: 532.1 and 534.1, found: 532.1 and 534.0.

4.2 | Pharmacological/biological assays

Radioligand displacement assays hD_2R and hD_3R have been performed as described previously, including modifications.[47] In short, the membrane was incubated with test ligands and [^{3}H]spiperone. Haloperidol was used to determine nonspecific binding. Assays were conducted in triplicate and in at least three separate experiments. Binding data were analyzed with GraphPad Prism using nonlinear regression. K_i values were obtained from IC_{50} values.[74]

4.3 | Molecular modeling

4.3.1 | Molecular docking

For molecular docking, GOLD 5.6.3 software was used.[75] All ligands were docked into cocrystal structures of D_2R (PDB ID: 6CM4) and D_3R (PDB ID: 3PBL). Protein preparation included the following steps: Lysozyme residues were removed manually and seven alanine residues were inserted using Modeler software[76]; hydrogen atoms were added to proteins using the PlayMolecule Protein Prepare procedure[77]; proteins were inserted in the POPC membrane using a membrane builder from CHARMM-GUI[78]; protein–ligand complexes were subjected to steepest decent energy minimization protocol in sander suite of Amber 2018 software[79] using Amber ff14sb and GAFF2 force fields.[80,81] Ligands for docking were prepared by the following procedure: For all compounds, selection of dominant microspecies at physiological pH 7.4 was performed using the Marvin Sketch 5.5.1.0 program. In the next step, the structures of all dominant forms were preoptimized with the semiempirical/PM3 (parameterized model revision 3) method.[59] The minimized structures were then refined by using a more precise quantum chemical Hartree–Fock/3-21G method[82] for geometry optimization employing Gaussian 09 software included in Chem3D Ultra 7 program. Docking procedure: The binding site was defined as residues within 6 Å from cocrystal ligands, and the number of genetic algorithm runs was set to 30, with maximum flexibility accounted for ligands. GoldScore was chosen as the scoring function, according to the lowest RMSD in redocking experiments and 2D interaction plots were generated using LigPlot+ software.[83]

4.3.2 | QM/MM calculations

Initial protein–ligand complexes were generated through molecular docking and prepared for simulation as explained above. The system was minimized and equilibrated through six steps using standard Amber inputs generated by CHARMM-GUI (see above). In each equilibration step, position restraints on protein were gradually reduced (starting from 10 kcal/mol/Å^2), whereas ligand's position restraints were kept constant (10 kcal/mol/Å^2) until the last two stages of equilibration. In the last two steps (ligand restraints = 10 kcal/mol/Å^2 and protein restraints = 0.5 kcal/mol/Å^2; ligand restraints = 0 kcal/mol/Å^2 and protein restraints = 0.1 kcal/mol/Å^2, respectively) of the equilibration protocol, QM/MM approach was used. QM/MM equilibration phase was performed using the sander suite of Amber 2018 utilizing semiempirical PM3 Hamiltonian for treatment of the QM region (ligand + residues located on a distance of 5 Å around the SF5 moiety, Figure S8), whereas the rest of the system was treated classically using Amber ff14sb. After equilibration, position restraints were completely removed and 100 ps of the production run was performed using the same protocol QM/MM (PM3). Each frame from the last 20 ps of trajectory was additionally minimized on the same semiempirical PM3 level and the complex with the minimal total energy was further optimized using QM/MM approach at the higher level of theory (DFT M06-2X functional with def2-TZUP basis set).[59,61] Each cycle of minimization consisted of 200 cycles of steepest descent and conjugated gradient. For the DFT QM/MM minimization, Orca 4.2.1 interfaced with the sander utility of Amber 2018 was used.[84,85] These simulations were treated nonperiodically with an electronic embedding scheme. The SHAKE algorithm was applied on H atoms in the QM region and the PME approach was used to calculate long-range electrostatics.

4.3.3 | NCI calculations

NCIplot 4.0 software[86] was used to interpret interactions between ligand **7i** and D_2R and D_3R. The NCI approach is based on the analysis of reduced density gradients (s). Reduced density gradient, given by

Equation (1), represents a simple function of electron density (ρ) and its gradient. It reflects local inhomogeneity of the electron density through points of space. In regions far from the molecule, in which the density decays to zero exponentially, the reduced gradient will have very large positive values. However, values of RDS approach zero in the cases of covalent bonds and NCIs. Lower densities and smaller gradients are usually associated with the NCIs, and higher densities and smaller gradients correspond to the covalent bonds:

$$s(r) = \frac{1}{C_s}\frac{|\nabla\rho(r)|}{\rho(r)^{4/3}}. \quad (1)$$

From a practical point of view, NCIplot analyzes only domains of weak electron density and low reduced density gradients (NCIs). Types of NCIs (hydrogen bond, van der Waals interactions, or steric clashes) are determined using Laplacian of the density. Namely, the sign of the second eigenvalues of the Hessian matrix ($\lambda 2$) can discriminate between different NCIs. The negative sign $\lambda 2$ with higher ρ values (>0.01 a.u.) usually corresponds to the strong stabilizing interactions (e.g., hydrogen bonds), whereas positive $\lambda 2$ and ρ values > 0.01 a.u. usually correspond to strong repulsive interactions. ρ values around 0 correspond to delocalized weak interactions (e.g., van der Waals interactions). Around zero, the sign of $\lambda 2$ is unstable and does not reflect the stabilizing or destabilizing nature of such interactions. Higher density corresponds to the stronger interactions (stabilizing or destabilizing, depending on the sign of $\lambda 2$) and vice versa. NCIs were analyzed in the terms of the 2D NCI plots of s versus $\rho \times \text{sign}\lambda 2$, 3D NCI plots (isosurfaces), and integrals of electron density ($\int\rho^2$). The cut-off value of $s \leq 0.3$ was used to plot gradients in 3D space and to generate isosurfaces of well-defined density values. Considering higher computational time required for calculation of NCI from SCF calculations (QM/MM), SCF-derived gradients were used to specifically access interactions of SF5 moiety with protein residues and to compare results with a computationally cheaper promolecular approach. The promolecular approach was further used to access interactions of whole ligands with proteins. Integrals of promolecular densities ($\int\rho^2$) of three specific regions, sign($\lambda 2$)$\rho(r)$ between −0.05 and −0.01; sign($\lambda 2$)$\rho(r)$ between −0.01 and 0.01, and sign($\lambda 2$)$\rho(r)$ between 0.01 and 0.05, across QM/MM trajectory were used to quantitatively access convergence of QM/MM simulations.[87,88]

ACKNOWLEDGMENTS

The authors would like to express their gratitude to the German Academic Exchange Service (Deutscher Akademischer Austauschdienst) for Milica Elek. They would like to thank the European Cooperation in Science and Technology (COST) COST Actions CA15135, CA18133, CA18240, and German Research Foundation (Deutsche Forschungsgemeinschaft-DFG: INST 208/664-1 FUGG) for financial support. Numerical simulations were run on the PARADOX-IV supercomputing facility at the Scientific Computing Laboratory, National Center of Excellence for the Study of Complex Systems, Institute of Physics Belgrade, supported in part by the Ministry of Education, Science, and Technological Development of the Republic of Serbia. Nemanja Djokovic, Slavica Oljacic, and Katarina Nikolic acknowledge the Ministry of Science and Technological Development of the Republic of Serbia, Faculty of Pharmacy UB Contract No. 451-03-68/2020-14/200161.

CONFLICTS OF INTEREST

The authors declare that there are no conflicts of interest.

ORCID

Milica Elek https://orcid.org/0000-0002-9094-8991
Nemanja Djokovic https://orcid.org/0000-0001-9972-3492
Annika Frank https://orcid.org/0000-0002-1637-2699
Slavica Oljacic https://orcid.org/0000-0001-9128-6072
Aleksandra Zivkovic https://orcid.org/0000-0001-5034-7916
Katarina Nikolic https://orcid.org/0000-0002-3656-9245
Holger Stark https://orcid.org/0000-0003-3336-1710

REFERENCES

[1] A. Carlsson, M. Lindqvist, T. Magnusson, B. Waldeck, *Science* **1958**, *127*, 471.
[2] O. Resnick, F. Elmadjian, *J. Clin. Endocrinol. Metab.* **1957**, 28.
[3] E. H. Labrosse, J. Axerod, S. Kety, *Science* **1958**, *26*, 7.
[4] M. Huotari, J. A. Gogos, M. Karayiorgou, O. Koponen, M. Forsberg, A. Raasmaja, J. Hyttinen, P. T. Ma, *Eur. J. Neurosci.* **2002**, *15*, 246.
[5] J. Smythies, *Biochim. Biophys. Acta* **1998**, *1380*, 159.
[6] D. R. Sibley, F. J. Monsma, *Trends Pharmacol. Sci.* **1992**, *13*, 61.
[7] P. H. Andersen, J. A. Gingrich, M. D. Bates, A. Dearry, P. Falardeau, S. E. Senogles, M. G. Caron, *Trends Pharmacol. Sci.* **1990**, *11*, 231.
[8] O. Civelli, J. R. Bunzow, D. K. Grandy, *Annu. Rev. Pharmacol. Toxicol.* **1993**, *33*, 281.
[9] S. Maramai, S. Gemma, S. Brogi, G. Campiani, S. Butini, H. Stark, M. Brindisi, *Front. Neurosci.* **2016**, *10*, 451.
[10] V. T. Seeman, *Trends Pharmacol. Sci.* **1994**, *15*, 4.
[11] D. Vallone, R. Picetti, E. Borrelli, *Neurosci. Biobehav. Rev.* **2000**, *24*, 125.
[12] N. M. Urs, S. M. Peterson, M. G. Caron, *Biol. Psychiatry* **2017**, *81*, 78.
[13] G. R. Beaulieu JM, *Pharmacol. Rev.* **2008**, *50*, 143.
[14] Y. Miyamoto, S. Katayama, N. Shigematsu, A. Nishi, T. Fukuda, *Brain Struct. Funct.* **2018**, *223*, 4275.
[15] C. de Mei, M. Ramos, C. Iitaka, *Curr. Opin. Pharmcol.* **2009**, *9*, 53.
[16] D. Gagnon, S. Petryszyn, M. G. Sanchez, C. Bories, J. M. Beaulieu, Y. de Koninck, A. Parent, M. Parent, *Sci. Rep.* **2017**, *7*, 1.
[17] D. Elgueta, M. S. Aymerich, F. Contreras, A. Montoya, M. Celorrio, E. Rojo-Bustamante, E. Riquelme, H. González, M. Vásquez, R. Franco, R. Pacheco, *Neuropharmacology* **2017**, 113110.
[18] A. E. Moritz, R. B. Free, D. R. Sibley, *Cell. Signal.* **2018**, *41*, 75.
[19] F. Boeckler, H. Lanig, P. Gmeiner, *J. Med. Chem.* **2005**, *48*, 694.
[20] L. Shi, J. A. Javitch, *Annu. Rev. Pharmacol. Toxicol.* **2002**, *42*, 437.
[21] E. Y. T. Chien, W. Liu, Q. Zhao, V. Katritch, G. W. Han, M. A. Hanson, L. Shi, A. H. Newman, J. A. Javitch, V. Cherezov, R. C. Stevens, *Science* **2010**, *330*, 1091.
[22] S. Wang, T. Che, A. Levit, B. K. Shoichet, D. Wacker, B. L. Roth, *Nature* **2018**, *555*, 269.
[23] P. Sokoloff, B. le Foll, *Eur. J. Neurosci.* **2017**, *45*, 2.
[24] A. H. Newman, P. Grundt, M. A. Nader, *J. Med. Chem.* **2005**, *48*, 366.
[25] G. A. Prieto, *J. Cent. Nerv. Syst. Dis.* **2017**, *9*, 177.
[26] P. Yang, J. S. Perlmutter, T. L. S. Benzinger, J. C. Morris, J. Xu, *Ageing Res. Rev.* **2020**, *57*, 100994.

[27] B. Landwehrmeyer, G. Mengod, J. M. Palacios, *Mol. Brain Res.* **1993**, *18*, 187.
[28] A. Kim, R. Nigmatullina, Z. Zalyalova, N. Soshnikova, A. Krasnov, *Mol. Neurobiol.* **2019**, *56*, 3437.
[29] A. E. Hackling, H. Stark, *ChemBioChem* **2002**, *3*, 946.
[30] S. Singh, A. Bali, T. Peshin, *Med. Chem.* **2020**, *16*, 1.
[31] A. F. Brito, L. K. S. Moreira, R. Menegatti, E. A. Costa, *Fundam. Clin. Pharmacol.* **2019**, *33*, 13.
[32] A. de Simone, D. Russo, G. F. Ruda, A. Micoli, M. Ferraro, R. M. C. Di Martino, G. Ottonello, M. Summa, A. Armirotti, T. Bandiera, A. Cavalli, G. Bottegoni, *J. Med. Chem.* **2017**, *60*, 2287.
[33] A. Loebel, L. Citrome, *BJPsych Bull.* **2015**, *39*, 237.
[34] É. Ágai-csongor, G. Domány, K. Nógrádi, J. Galambos, I. Vágó, I. Greiner, I. Laszlovszky, A. Gere, É. Schmidt, B. Kiss, M. Vastag, K. Tihanyi, K. Sághy, J. Laszy, I. Gyertyán, M. Zájer-balázs, L. Gémesi, M. Kapás, Z. Szombathelyi, *Bioorg. Med. Chem. Lett.* **2012**, *22*, 3437.
[35] R. H. Campbell, M. Diduch, K. N. Gardner, C. Thomas, *Ment. Health Clin.* **2017**, *7*, 1.
[36] K. P. Garnock-jones, *CNS Drugs* **2017**, *31*, 513.
[37] H. Lavreysen, X. Langlois, A. Ahnaou, W. Drinkenburg, P. Riele, I. Biesmans, I. Van Der Linden, L. Peeters, A. Megens, C. Wintmolders, J. M. Cid, A. A. Trabanco, J. I. Andrés, F. M. Dautzenberg, R. Lütjens, G. Macdonald, J. R. Atack, *J. Pharmacol. Exp. Ther.* **2013**, *316*, 514.
[38] M. Nakamura, *U.S. Patent: US9815827*, **2017**.
[39] F. J. Garcia-Ladona, B. F. Cox, *CNS Drug Rev.* **2003**, *9*, 141.
[40] Z. X. Xi, E. L. Gardner, *CNS Drug Rev.* **2007**, *13*, 240.
[41] M. D. Wood, I. Boyfield, D. J. Nash, F. R. Jewitt, K. Y. Avenell, G. J. Riley, *CNS Drug Rev.* **2000**, *47*, 141.
[42] A. H. Newman, T. Beuming, A. K. Banala, P. Donthamsetti, K. Pongetti, A. Labounty, B. Levy, J. Cao, M. Michino, R. R. Luedtke, J. A. Javitch, L. Shi, *J. Med. Chem.* **2013**, *55*, 6689.
[43] V. Kumar, A. E. Moritz, T. M. Keck, A. Bonifazi, M. P. Ellenberger, C. D. Sibley, R. B. Free, L. Shi, J. R. Lane, D. R. Sibley, A. H. Newman, *J. Med. Chem.* **2017**, *60*, 1478.
[44] S. Vangveravong, Z. Zhang, M. Taylor, M. Bearden, J. Xu, J. Cui, W. Wang, R. R. Luedtke, R. H. MacH, *Bioorg. Med. Chem.* **2011**, *19*, 3502.
[45] N. Vida, J. Vaclavík, P. Beier, *Beilstein J. Org. Chem.* **2016**, *12*, 110.
[46] P. Das, E. Tokunaga, N. Shibata, *Tetrahedron Lett.* **2017**, *58*, 4803.
[47] M. F. Sowaileh, R. A. Hazlitt, D. A. Colby, *ChemMedChem* **2017**, *12*, 1481.
[48] M. Schübler, B. Sadek, T. Kottke, L. Weizel, H. Stark, *Front. Chem.* **2017**, *5*, 64.
[49] L. Stank, A. Frank, S. Hagenow, H. Stark, *MedChemComm* **2019**, *10*, 1926.
[50] A. Frank, D. J. Kiss, G. M. Keserű, H. Stark, *Sci. Rep.* **2018**, *8*, 1.
[51] N. Griffon, C. Pilon, F. Sautel, J. C. Schwartz, P. Sokoloff, *J. Neural Transm.* **1996**, *103*, 1163.
[52] J. R. Wagner, C. P. Churas, S. Liu, R. V. Swift, M. Chiu, C. Shao, V. A. Feher, S. K. Burley, M. K. Gilson, R. E. Amaro, *Structure* **2019**, *27*, 1326.
[53] S. Ananthan, S. K. Saini, G. Zhou, J. V. Hobrath, I. Padmalayam, L. Zhai, J. R. Bostwick, T. Antonio, M. E. A. Reith, S. McDowell, E. Cho, L. McAleer, M. Taylor, R. R. Luedtke, *J. Med. Chem.* **2014**, *57*, 7042.
[54] N. Ferruz, S. Doerr, M. A. Vanase-Frawley, Y. Zou, X. Chen, E. S. Marr, R. T. Nelson, B. L. Kormos, T. T. Wager, X. Hou, A. Villalobos, S. Sciabola, G. de Fabritiis, *Sci. Rep.* **2018**, *8*, 1.
[55] Z. Wang, H. Sun, X. Yao, D. Li, L. Xu, Y. Li, S. Tian, T. Hou, *Phys. Chem. Chem. Phys.* **2016**, *18*, 12964.
[56] L. Fan, L. Tan, Z. Chen, J. Qi, F. Nie, Z. Luo, J. Cheng, S. Wang, *Nat. Commun.* **2020**, *11*, 1.
[57] S. Gadhiya, P. Cordone, R. K. Pal, E. Gallicchio, L. Wickstrom, T. Kurtzman, S. Ramsey, W. W. Harding, *ACS Med. Chem. Lett.* **2018**, *9*, 990.
[58] J. Z. Penjišević, D. B. Andrić, V. B. Šukalović, G. M. Roglić, V. Šoškić, S. V. Kostić-Rajačić, *J. Serbian Chem. Soc.* **2019**, *84*, 925.
[59] Y. Zhao, D. G. Truhlar, *Theor. Chem. Acc.* **2008**, *120*, 215.
[60] J. J. P. Stewart, *J. Comput. Chem.* **1989**, *10*, 209.
[61] F. Weigend, R. Ahlrichs, *Phys. Chem. Chem. Phys.* **2005**, *7*, 3297.
[62] A. Li, H. S. Muddana, M. K. Gilson, *J. Chem. Theory Comput.* **2014**, *10*, 1563.
[63] C. Dalvit, A. Vulpetti, *ChemMedChem* **2011**, *6*, 1044.
[64] D. Lachmann, C. Studte, B. Männel, H. Hübner, P. Gmeiner, B. König, *Chem. A Eur. J.* **2017**, *23*, 13423.
[65] A. S. Pirzer, R. Lasch, H. Friedrich, H. Hu, P. Gmeiner, M. R. Heinrich, *J. Med. Chem.* **2019**, *62*, 9658.
[66] A. Hackling, R. Ghosh, S. Perachon, A. Mann, H. D. Höltje, C. G. Wermuth, J. C. Schwartz, W. Sippl, P. Sokoloff, H. Stark, *J. Med. Chem.* **2003**, *46*, 3883.
[67] M. Khatri, S. K. Rai, R. Ranbhor, K. Kishore, M. Tiwari, *Pharmacol. Res.* **2012**, *35*, 1143.
[68] M. Jean, J. Renault, N. Levoin, D. Danvy, T. Calmels, I. Berrebi-Bertrand, P. Robert, J. C. Schwartz, J. M. Lecomte, P. Uriac, M. Capet, *Bioorg. Med. Chem. Lett.* **2010**, *20*, 5376.
[69] M. Résimont, R. J. F. Liégeois, *Bioorg. Med. Chem. Lett.* **2010**, *20*, 5199.
[70] M. Muñoz-Osses, F. Godoy, A. Fierro, A. Gómez, N. Metzler-Nolte, *Dalt. Trans.* **2018**, *47*, 1233.
[71] X. A. Dominguez, I. C. Lopez, R. Franco, *J. Org. Chem.* **1961**, *26*, 1625.
[72] P. Chen, M. Taylor, S. A. Griffin, A. Amani, H. Hayatshahi, K. Korzekwa, M. Ye, R. H. Mach, J. Liu, R. R. Luedtke, J. C. Gordon, B. E. Blass, *Bioorg. Med. Chem. Lett.* **2019**, *29*, 2690.
[73] M. Leopoldo, E. Lacivita, P. de Giorgio, N. A. Colabufo, M. Niso, F. Berardi, R. Perrone, *J. Med. Chem.* **2006**, *49*, 358.
[74] C. Yung-Chi, W. H. Prusoff, *Biochem. Pharmacol.* **1973**, *22*, 3099.
[75] G. Jones, P. Willet, R. C. Glen, A. R. Leach, R. Taylor, *J. Mol. Biol.* **1997**, *267*, 727.
[76] B. Webb, A. Sali, *Curr. Protoc. Bioinf.* **2016**, *54*, 5.6.1.
[77] G. Martínez-Rosell, T. Giorgino, G. de Fabritiis, *J. Chem. Inf. Model.* **2017**, *57*, 1511.
[78] J. Lee, X. Cheng, J. M. Swails, M. S. Yeom, P. K. Eastman, J. A. Lemkul, S. Wei, J. Buckner, J. C. Jeong, Y. Qi, S. Jo, V. S. Pande, D. A. Case, C. L. Brooks, A. D. MacKerell, J. B. Klauda, W. Im, *J. Chem. Theory Comput.* **2016**, *12*, 405.
[79] D. A. Case, R. C. Walker, T. E. Cheatham, A. Roitberg, K. M. Merz, R. Luo, T. Darpen, J. Wang, R. E. Duke, D. R. Roe, S. LeGrand, J. Swails, A. W. Götz, J. Smith, D. Cerutti, S. R. Brozell, T. Luchko, L. Wilson, R. Krasny, V. Man, V. W. D. Cruzeiro, D. Ghoreishi, G. Monard, C. Sagui, F. Pan, G. A. Cisneros, Y. Miao, J. Shen, R. Harris, Y. Huang, C. Lin, D. J. Mermelstein, P. Li, A. Onufriev, Y. Xiong, S. Izadi, R. M. Wolf, X. Wu, H. Gohlke, S. Schott-Verdugo, R. Qi, L. Xiao, H. Wei, D. Greene, T. Lee, T. Geise, G. Giambasu, D. York, J. Liu, H. Nguyen, A. Kovalenko, M. Gilson, I. Ben-Shalom, C. Nguyen, T. Kurtzman, P. A. Kollman, et al., *AMBER 2019*, University of California, San Francisco, CA **2019**.
[80] J. A. Maier, C. Martinez, K. Kasavajhala, L. Wickstrom, K. E. Hauser, C. Simmerling, *J. Chem. Theory Comput.* **2015**, *11*, 3696.
[81] D. Vassetti, M. Pagliai, P. Procacci, *J. Chem. Theory Comput.* **2019**, *15*, 1983.
[82] W. J. Hehre, L. Radom, P. v. R. Schleyer, J. A. Pople, *Ab Initio Molecular Orbital Theory*, John Wiley, New York, NY **1986**.
[83] R. A. Laskowski, M. B. Swindells, *J. Chem. Inf. Model.* **2011**, *51*, 2778.
[84] F. Neese, *Wiley Interdiscip. Rev.: Comput. Mol. Sci.* **2018**, *8*, 4.

[85] An extenible interface for QM/MM molecular dynamics with AMBER-Abstract
[86] J. Contreras-García, E. R. Johnson, S. Keinan, R. Chaudret, J. P. Piquemal, D. N. Beratan, W. Yang, *J. Chem. Theory Comput.* **2011**, *7*, 625.
[87] R. Chaudret, B. de Courcy, J. Contreras-García, E. Gloaguen, A. Zehnacker-Rentien, M. Mons, J. P. Piquemal, *Phys. Chem. Chem. Phys.* **2014**, *16*, 9876.
[88] R. Laplaza, F. Peccati, R. A. Boto, C. Quan, A. Carbone, J. P. Piquemal, Y. Maday, J. Contreras-García, *Wiley Interdiscip. Rev.: Comput. Mol. Sci.* **2020**, e1497.

SUPPORTING INFORMATION

Additional supporting information may be found online in the supporting information tab for this article.

How to cite this article: M. Elek, N. Djokovic, A. Frank, S. Oljacic, A. Zivkovic, K. Nikolic, H. Stark, *Arch. Pharm.* **2021**, e2000486.